

# Crystallization mechanisms occurring in the Se–Te glassy system

Roman Svoboda · Jiří Málek

Received: 4 February 2014 / Accepted: 22 September 2014 / Published online: 2 October 2014  
© Akadémiai Kiadó, Budapest, Hungary 2014

**Abstract** Crystallization kinetics, studied under non-isothermal conditions in dependence on particle size, is reviewed for the Se–Te glassy system, with particular focus on occurring macroscopic crystallization mechanisms. The observed complexity of the crystallization processes is explained in terms of the two previously identified mechanisms—bulk crystallization originating from nuclei randomly distributed in the volume of each glass particle (formation of these nuclei is consistent with the classical nucleation theory) and crystallization from surface/volume active centers, dislocations, structural defects, and heterogeneities originating from the mechanical damage of the material (e.g., during grinding and milling). In addition, a new crystallization mechanism, previously unobserved in this system, was revealed for hyperquenched  $\text{Se}_{95}\text{Te}_5$  glass. The origin of this mechanism is suggested to be closely associated with the stress-induced defects contained in the highly strained structure of this glass. The strong compositional dependence of the occurrence of this mechanism then seems to be caused by the high cooperativity of the amorphous structure of the specific composition.

**Keywords** Crystallization mechanism · DSC · JMA model ·  $\text{Se}_{(1-x)}\text{Te}_x$

## Introduction

Recently, extensive systematic research dealing with macroscopic crystallization in Se–Te glasses was conducted [1–7]. Two novel methodologies for treating the crystallization data measured by differential scanning calorimetry (DSC) were developed within the framework of these studies. Based on the advanced interpretation of characteristic kinetic functions  $z(\alpha)$  and  $y(\alpha)$  the complexity of the respective crystallization processes was revealed and identified. In this regard, it was found that the considered compositional set of Se–Te glasses is actually a very good model system for studying complex crystallization processes composed of overlapping surface and bulk crystallization mechanisms. More precisely, the two involved mechanisms were identified as: bulk crystallization originating from nuclei randomly distributed in the volume of each glass particle (formation of these nuclei is consistent with the classical nucleation theory), and crystallization from surface/volume active centers, dislocations, structural defects, and heterogeneities. The latter was originally denoted as “surface” crystallization; however, a similar mechanism can also be associated with crystallization from microstructural heterogeneities and mechanically induced defects in the bulk material.

The first approach [2, 8] to the advanced interpretation of system complexity is based on the introduction of different amounts and ratios of the two above-mentioned crystallization centers (bulk and “surface”) into the material, and studying the thermally activated crystallization response. In practice, this is realized by preparation of a set of powder fractions divided by particle size, where the continued (more intensive) grinding procedure corresponds to larger amounts of heterogeneities and stress introduced into the sample (lower size of powder grains also implies a

R. Svoboda (✉) · J. Málek  
Department of Physical Chemistry, Faculty of Chemical  
Technology, University of Pardubice, Studentska 573,  
Pardubice 532 10, Czech Republic  
e-mail: roman.svoboda@upce.cz

larger portion of the material containing mechanically induced defects and stress). In case of sufficiently narrow particle size fraction intervals, a continuously changing ratio between the densities of the two respective types of nucleation centers is obtained. Applying non-isothermal heating scans then provokes simultaneous manifestation of the two crystallization mechanisms, resulting in overlapping DSC peaks with correspondingly changing intensity. In addition, application of various heating rates further diversifies the crystallization response—magnitude, shape, and relative proportion of the respective DSC peaks. Comparison of the kinetic evaluations (most importantly the shape of the characteristic kinetic functions) undertaken for the respective powder fractions then provides extensive information about the nature, origin, and characteristics of the process complexity.

The second approach to the description of the crystallization complexity is then based on the actual separation of the identified crystallization mechanisms. For this reason, the modified Fraser–Suzuki deconvolution methodology was recently developed [5]. For accurate and physically meaningful deconvolution, maximum information about the involved processes should be gained prior to the actual separation. The information obtained within the advanced interpretation of characteristic kinetic functions may be effectively utilized in this regard. This approach, with very good results, was applied in cases of pure amorphous selenium and several chosen particle size fractions of the  $\text{Se}_{90}\text{Te}_{10}$  and  $\text{Se}_{70}\text{Te}_{30}$  compositions [5–7].

High consistency, reproducibility, and coherency of the results of all the above-mentioned studies may lead to the conclusion that, by performing the particle-size-based study to the given extent, the maximum range of process complexity is achieved and, hence, the complete description of the crystallization behavior in the studied glassy system is obtained in terms of the two above-mentioned crystallization mechanisms. However, our recent data for the  $\text{Se}_{95}\text{Te}_5$  chalcogenide composition revealed the presence of a possible third type of crystallization mechanism. In the current article, this finding will be explored in greater detail.

## Experimental

Experimental details on the preparation and measurements of the  $\text{Se}$ ,  $\text{Se}_{90}\text{Te}_{10}$ ,  $\text{Se}_{80}\text{Te}_{20}$ , and  $\text{Se}_{70}\text{Te}_{30}$  compositions can be found in the, respective, previously published papers [1–7]. In addition to these materials, a new glass with  $\text{Se}_{95}\text{Te}_5$  composition was prepared. Preparation of this glass was performed by means of the classical melt-quenching technique, where two distinct methods are applied. In the case of both batches, pure (5N) elements

were accurately weighed into quartz ampoules, held in a rocking furnace for 48 h for the melt to react and homogenize and then quenched in water. The first batched ampoule was annealed at 650 °C and the quench was realized in the maximum possible way—this glass will be denoted as “batch a).” On the other hand, the second ampoule was annealed at 350 °C and after unloading from the furnace the melt was allowed to cool for approximately 10 s in air before quenching in water—glass prepared in this way will be denoted as “batch b).”

The amorphous nature of each glass was checked by X-ray diffraction, Bruker AXS diffractometer D8 Advance equipped with a horizontal goniometer and scintillation counter utilizing  $\text{CuK}_\alpha$  radiation was used in this regard. Homogeneity of the glasses was verified from the position of the relaxation peak at  $T_g$ , which was measured under defined thermal history for samples taken randomly from the bulk glass. Each prepared glass was ground to a set of powders with defined particle sizes: 0–20, 20–50, 50–125, 125–180, 180–250, 250–300, and 300–500  $\mu\text{m}$  (the grinding was performed in an agate mortar for approx. 30 s). Additionally, bulk samples were prepared by cracking a thin layer of as-prepared bulk glass. In the case of the powders, a thin layer of the material was spread on the bottom of T-zero aluminum pans to improve thermal contact; masses of the samples varied between 8 and 10 mg.

Crystallization behavior of the prepared glasses was studied using a conventional DSC Q2000 (TA Instruments) equipped with cooling accessory, autolid, autosampler, and T-zero Technology. Dry nitrogen was used as the purge gas at a rate of 50  $\text{cm}^3 \text{min}^{-1}$ . The calorimeter was calibrated through the use of melting temperatures of In, Zn, and  $\text{H}_2\text{O}$ . The zero-line course was checked daily. With regard to the specific thermal history, each sample was first stabilized at 55 °C for 5 min (for the glass structure to stabilize in the undercooled liquid region; this isotherm also served as a pre-nucleation period), then the sample was cooled at 10 °C  $\text{min}^{-1}$  to 30 °C and the measuring heating scan was applied immediately. Heating rates applied during the heating scans varied from 0.5 to 30 °C  $\text{min}^{-1}$ . Each measurement was reproduced twice in order to estimate the experimental errors; spline baselines were used for imitation of the thermokinetic background. Nearly perfect reproducibility of the data acquired within each respective batch was achieved.

In Fig. 1 an exemplary comparison of the full DSC curves measured for the two studied glass batches is shown—data for similar particle size fractions and applied heating rates are displayed. As can be seen, the curves very well overlap in the glass transition and melting regions; the crystallization effect, on the other hand, differs markedly. In the inset the glass transition region is magnified,

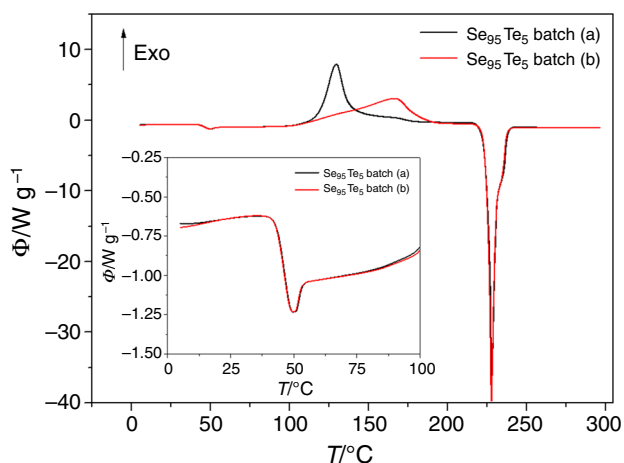


**Fig. 1** Example DSC curves measured for the two prepared glass batches (data for similar particle size fraction and heating rate are displayed). Zoomed glass transition region is shown in the inset

showing perfect overlay of the two curves and no signs of “double  $T_g$ ”, which would suggest phase separation. The glass transition midpoint is  $46.3 \pm 0.1$  °C. Regarding the melting region, both materials again show similar characteristic features—namely the high-temperature shoulder suggesting melting of two crystalline “phases” (the surface and bulk crystals). Temperature onset of the melting peak occurs at 225 °C. Similarity of the melting peaks then confirms similar nature of the crystalline products despite the obviously differing mechanisms of their formation—this will be referred to later.

## Results and discussion

In the first part of the “Results and discussion” section, the new crystallization mechanism occurring in the  $\text{Se}_{95}\text{Te}_5$  glass will be identified and a qualitative evaluation of its properties will be undertaken. Consequently, in the second part, this newly identified crystallization behavior will be treated quantitatively by means of standard kinetic analysis—the difficulty of its interpretation in the case of highly pronounced process complexity will be discussed. In the last part, the structural origin of the compositionally anomalous occurrence of this crystallization mechanism will be proposed.

### Shapes of $\text{Se}_{95}\text{Te}_5$ crystallization peaks and their interpretation

Crystallization behavior in  $\text{Se}_{95}\text{Te}_5$  glass was closely examined by means of a DSC particle size dependent study for the two prepared batches of glass (a) and (b). In Fig. 2a the DSC data for low heating rates ( $0.5\text{--}7$  °C  $\text{min}^{-1}$ ) are

compared for the two prepared batches—examples of fine, middle-sized, and coarse particle size fractions were chosen to make the comparison. In Fig. 2a it can be seen that the shape of the crystallization peaks is strikingly different for the two prepared batches. In the case of batch (a) the peaks are sharp with elongated tails, while in the case of batch (b) the peaks are more or less symmetric with a rather slower increase in the initial peak edge. Another very interesting fact is associated with the location of the crystallization peaks with respect to the temperature axis compared for different powder fractions. In the case of batch (a) the peaks show almost no shift in temperature with increasing particle size (which is quite unusual considering the so far observed behavior in the Se–Te glassy system [1–7]), while for batch (b) the crystallization peaks shift to higher temperatures with increasing grain size.

To explain the marked difference in the crystallization behavior of the two compositionally identical prepared batches of  $\text{Se}_{95}\text{Te}_5$  glass, the microstructural aspect needs to be considered. From the compositional point of view, the microstructure of both glass batches should be identical: eventual slight differences in bond arrangements or Se–Te chain lengths caused by the different structure of the original liquid are usually erased closely above  $T_g$ ; in addition, the structural relaxation kinetics reflecting the molecular structure seems to be identical for the two prepared batches—inset in Fig. 1 demonstrates the perfect overlap of the glass transition data for the two batches. To further confirm the similarity of relaxation kinetics, the so-called intrinsic relaxation cycles [9–11] were performed and the apparent activation energy of structural relaxation was evaluated for both glass batches: batch (a)  $\Delta h^* = 316 \pm 8$  kJ  $\text{mol}^{-1}$  and batch (b)  $\Delta h^* = 318 \pm 20$  kJ  $\text{mol}^{-1}$ . Different compositional phase separation and formation of different microstructural regions can also be ruled out due to the similarity of the relaxation peak shape at glass transition (which is usually very sensitive to all separation processes)—see inset in Fig. 1—as well as due to the well known absolute mixing of the Se and Te elements. On the other hand, considering the density/defects microstructural aspect, the two glasses are markedly different. In the case of the glass rapidly cooled from high temperature batch (a) large amount of stress-induced defects is formed within the material structure due to the fast and large change in volume during the quench leading to high level of strain. In the case of the significantly lower annealing temperature applied to batch (b) before the quench, the associated volumetric change was significantly smaller and the glass microstructure is a lot closer to the ideally packed conformation, corresponding to the extrapolated pseudo-equilibrium curve of undercooled liquid—i.e., significantly lower amount of stress-induced defects is formed.

Based on the latter, the interpretations introduced for the formerly studied compositions [1–7] can be extended for

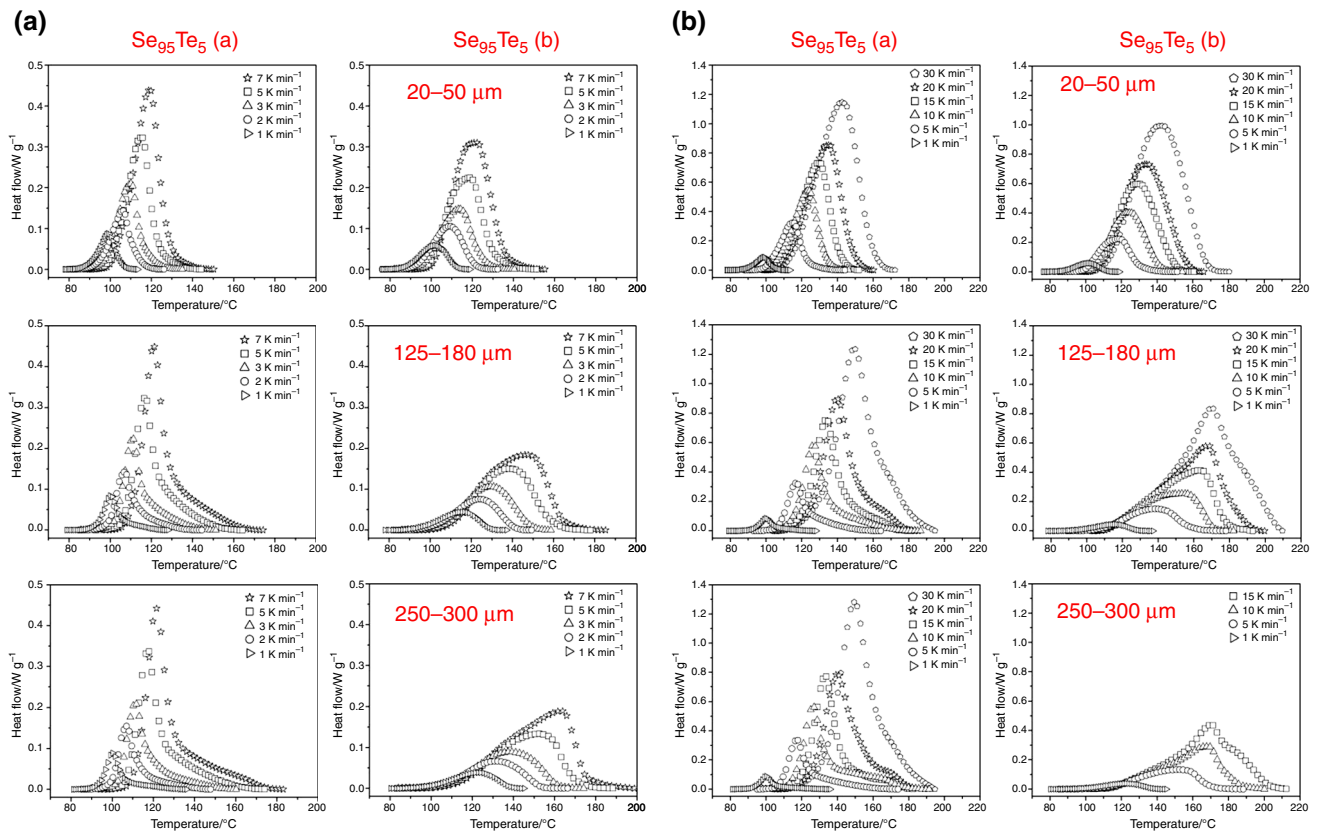


**Fig. 2** Crystallization peaks corresponding to non-isothermal measurements of chosen particle size fractions of the  $\text{Se}_{95}\text{Te}_5$  glass—particular rows match the individual studied fractions. In the left part **a** the data for low heating rates are displayed; right part **b** contains

data for high heating rates. In each part respective columns corresponding to the data for batches (a) and (b) are shown. Exotherms manifest in upward direction

the current  $\text{Se}_{95}\text{Te}_5$  material. The well-established conception of surface/volume crystallization complexity can be applied in the following way. Starting with batch (b) corresponding to “commonly” quenched glass with a high portion of relaxed bulk material, it is apparent that the overall crystallization peak lowers and broadens with increasing particle size. This implies dominance of the surface/heterogeneities originating crystallization mechanism. In addition, the deformation of the peak shape progressing with increasing heating rate and particle size, as well as the shift in the crystallization peaks toward higher temperatures with increasing particle size, both suggest simultaneous manifestation of the crystallization processes originating from surface/heterogeneities and common bulk-located nuclei. Finally, the changing shape of the peaks corresponds to the gradually developing ratio between the manifestation intensity of the two involved crystallization mechanisms. Similar behavior is described e.g., for pure Se [6, 7] or  $\text{Se}_{90}\text{Te}_{10}$  and  $\text{Se}_{80}\text{Te}_{20}$  [5].

In contrast, in the case of batch (a), both the intensity and position with respect to the temperature axis do not change with particle size for the major peaks. Furthermore,

the general shape of the crystallization peaks does not change either with heating rate or particle size. Such behavior corresponds to the majority of the grain volume crystallizing by a similar mechanism, where neither the surface nor mechanically induced heterogeneities play a significant role (crystallization behavior would change with particle size). This well corresponds to the nucleation and the following crystal growth processes originating from the microstructural bulk stress-induced defects formed during the initial glass-formation procedure. This is in accordance with the observed peak shape, where the dominant part of the peak corresponds to the fast autocatalytic crystallization process in the grain bulk, while the peak tails correspond to substantially slower growth of the large and already touching crystallites filling the space between them.

The trends observed for the low heating rates are quite similar to those for higher heating rates, which are, however, further complicated by the effects of thermal gradients and the more pronounced manifestation of secondary crystallization processes with higher apparent activation energy (due to the energy surplus introduced during the

faster heating rates). DSC data for the three chosen particle sizes and high heating rates are shown in Fig. 2b.

To conclude, based on the shape of the DSC crystallization peaks of the hyperquenched  $\text{Se}_{95}\text{Te}_5$  glass, a new (in the Se–Te system so far unobserved) crystallization mechanism was found. The corresponding nucleation and consequent crystal growth seem to originate from the microstructural stress-induced defects formed within the material during glass-formation. The most important argument for the latter statement is the striking independence of the crystallization mechanisms from particle size distribution of the heated glass powder.

#### Quantitative kinetic analysis versus process complexity

In the previous section, the qualitative interpretation of crystallization complexity was undertaken for the two prepared glass batches. Quantitatively, the crystallization kinetics studied by DSC can be described by the following equation [12]:

$$\Phi = \Delta H \cdot A \cdot e^{-E/RT} \cdot f(\alpha) \quad (1)$$

where  $\Phi$  is the measured heat flow,  $\Delta H$  is the crystallization enthalpy,  $A$  is the pre-exponential factor,  $E$  is the apparent activation energy of the process,  $R$  is the universal gas constant,  $T$  is temperature, and  $f(\alpha)$  stands for an expression of a kinetic model with  $\alpha$  being conversion (the thermal inertia term characteristic for heat-flux DSCs can be in case of modern instruments safely neglected).

In the first step, the apparent activation energy is usually determined. In the case of complex processes it was shown that the original Kissinger equation [13] may, in certain ways, be superior to the isoconversion methods (which can be significantly influenced by various data-distortive effects) [2, 6, 14]. The Kissinger equation is expressed followingly:

$$\ln\left(\frac{q^+}{T_p^2}\right) = -\frac{E}{RT_p} + \text{const.} \quad (2)$$

where  $q^+$  is heating rate and  $T_p$  corresponds to the temperature of the maximum of the crystallization peak. The Kissinger plot, where the slope of the dependence is proportionate to the activation energy (in the case of these data ranging from  $123 \pm 2 \text{ kJ mol}^{-1}$  for finest powders to  $102 \pm 6 \text{ kJ mol}^{-1}$  for coarse powders; the error of  $E$  determination as well as the  $E$  values markedly depend on the selected data range, only data for low heating rates were evaluated in this case [6]), is, for all the measurable heating rates and particle size fractions of the two glass batches, shown in Fig. 3a. As can be seen, the data for batch (b) show commonly observed shifts and curvatures with changing temperature and heating rate, which indicate

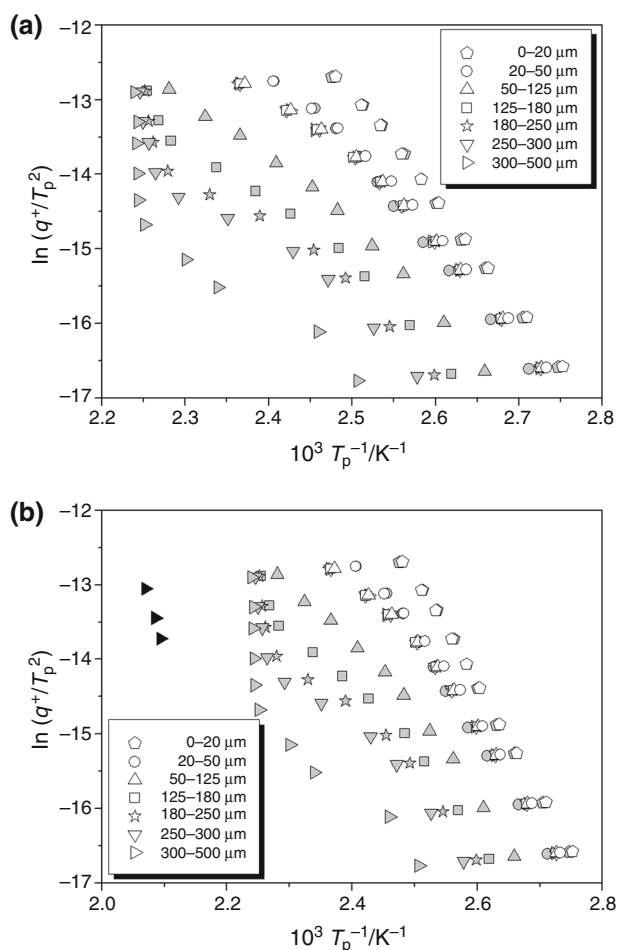


**Fig. 3** Determination of apparent activation energy of the crystallization process according to the Kissinger method for all studied  $\text{Se}_{95}\text{Te}_5$  particle size fractions. Empty symbols correspond to the hyperquenched glass (a), gray and black symbols represent the data for the normally quenched glass (b). The black symbols represent the high-temperature peak maxima in case of the differentiated double-peaks of the 300–500  $\mu\text{m}$  powder (see also Fig. 10). In graph a the low-temperature part of the data is enlarged; graph b shows the whole temperature range. Error of  $T_p$  determination is lower than the magnitude of the points

overlapping “surface”/bulk crystallization mechanism characteristics for Se–Te glasses. Incidentally, based on our other recent results, it seems that the curvatures [1–7] observed in the Kissinger plot for Se–Te coarse powders and bulks can be associated with the transition between the formation of two types of spherulitic crystallites (high-temperature type A and low-temperature type B) as identified by Ryschenkow and Faivre and Bisault, Ryschenkow, and Faivre [15, 16] for amorphous selenium. Considering the framework of the three types of crystallization mechanism occurring in Se–Te glasses, the two above-mentioned microscopic crystal growth patterns fall within the bulk crystallization mechanism originating from randomly dispersed nuclei. In addition, in the case of batch (b), the

data for the high heating rates of coarse powders show a sharp increase, which usually corresponds to the crystallization process being interrupted by the melting of the sample. However, in case of the  $\text{Se}_{95}\text{Te}_5$  material the onset of melting peak occurs at  $\sim 225$  °C (see Fig. 1), which is too far from the temperature to which the dependences in the Kissinger plot limit (approx. 170 °C). From Fig. 2b it is obvious that this convergence is caused by occurrence of an additional crystallization mechanism, which seems to be very narrowly localized in temperature. For the coarsest fraction two well-resolved maxima are apparent at high heating rates (one for the original “major” process and one for the new secondary crystallization peak), further confirming the occurrence of the temperature-localized secondary crystallization mechanism. The Kissinger plot upgraded with the new data corresponding to the original “major” crystallization process is shown in Fig. 3b. This finding will be further commented on in Section 3.3, where deconvolution of the respective processes will be performed.

A completely different situation arises in the case of the hyperquenched batch (a). As is already apparent from Fig. 2, the position of the crystallization peak does not change in temperature with increasing particle size. As can be seen, the corresponding activation energy is very similar to that obtained for the fine powders of batch (a) but does not change with particle size fraction (the exact values varying between 106 and 111  $\text{kJ mol}^{-1}$  and the average error being  $\pm 3$   $\text{kJ mol}^{-1}$ ). Interestingly, there is a striking resemblance in the position of the peak maxima on the temperature axis for the finest powders of the two glass batches. This should indicate either high involvement of the “surface”/heterogeneities crystallization mechanisms in the case of this fraction or high similarity of the two crystallization mechanisms (dominating for the respective glass batches)—based on the rest of the data, the former is a more probable case.

In the second step of the kinetic analysis, the crystallization model needs to be determined. For this task, the so-called characteristic kinetic functions  $z(\alpha)$  and  $y(\alpha)$  defined by Málek [17, 18] were found to be very suitable. The functions are based on a simple transformation of experimental data according to the following equations (non-isothermal conditions):

$$y(\alpha) = \Phi \cdot e^{E/RT} \quad (3)$$

$$z(\alpha) = \Phi \cdot T^2 \quad (4)$$

The data are plotted against  $\alpha$  and usually normalized on both axes for better clarity when comparing a whole set of curves measured at different heating rates. These functions provide an extensive amount of information on the origin and nature of crystallization complexity [2, 4, 6, 7];

however, they seem to have their limitations in the case of only partially overlapping processes. This can be seen in Fig. 4a, where the  $z(\alpha)$  functions calculated for the chosen particle size fractions are compared for the two prepared glass batches. It can be seen that, for a “consistent” peak with no major shoulders [data for batch (b)], the shape of the  $z(\alpha)$  function corresponds well to the Johnson–Mehl–Avrami (JMA) kinetics [19–22] for which the maximum of the  $z(\alpha)$  function occurs at  $\alpha \sim 0.63$  (the exceptions are the highest heating rates where the peaks are already severely deformed by the manifestation of the secondary crystallization process). In the case of batch (a), on the other hand, the shape of the  $z(\alpha)$  functions is markedly deformed due to the presence of pronounced shoulders (with the exception of the finest powders). As can be seen from the data for the finest powders of batch (a), the kinetics of the pure dominant peak is also very close to that of the JMA.

Similar conclusions can be drawn also for the  $y(\alpha)$  functions (chosen plots can be found in Fig. 4b), which usually contains information [2, 6, 8] about the detailed nature of the crystallization mechanism. The marked peak tails, occurring in the case of the data from batch (a), again distort the shape of the kinetic functions so that the kinetic information is lost. Again, only the data for the finest powders of batch (a) and the lower heating rates of batch (b) can be evaluated properly.

Summarized quantitative representation of the previous paragraph is depicted in the so-called kinetic plot—Fig. 5. The data, averaged over all applied heating rates, are shown for all studied particle size fractions of the two studied batches. Coarseness of the powders within each respective batch increases in the direction of the arrows. The original interval for applicability of the JMA model (as derived by Málek) is suggested in figure; however, as shown, for example, in [2, 4], this interval can be substantially extended while still obtaining a highly acceptable description by the JMA model. Data for batch (b) represent typical behavior corresponding to the “surface”/volume type of crystallization kinetics, where the autocatalytic crystal growth, originating from defects and heterogeneities, gradually vanishes with increasing particle size (a lower amount of crystallization centers is mechanically induced during powder grinding) and is replaced by the classical surface-nucleated growth from nuclei randomly dispersed in the bulk material of the glass grains, that is, the data in the kinetic plot shift toward the JMA behavior ( $\alpha_{\text{max},z} \sim 0.63$ ) with increasing particle size. On the other hand, in the case of batch (a) the data in the kinetic plot show exactly opposite behavior—only the finest powder corresponds to the JMA mechanism, while the increasing particle size causes increasing deviation from the model JMA crystallization behavior. The unchanging shape of the dominant part of the crystallization peak, together with its

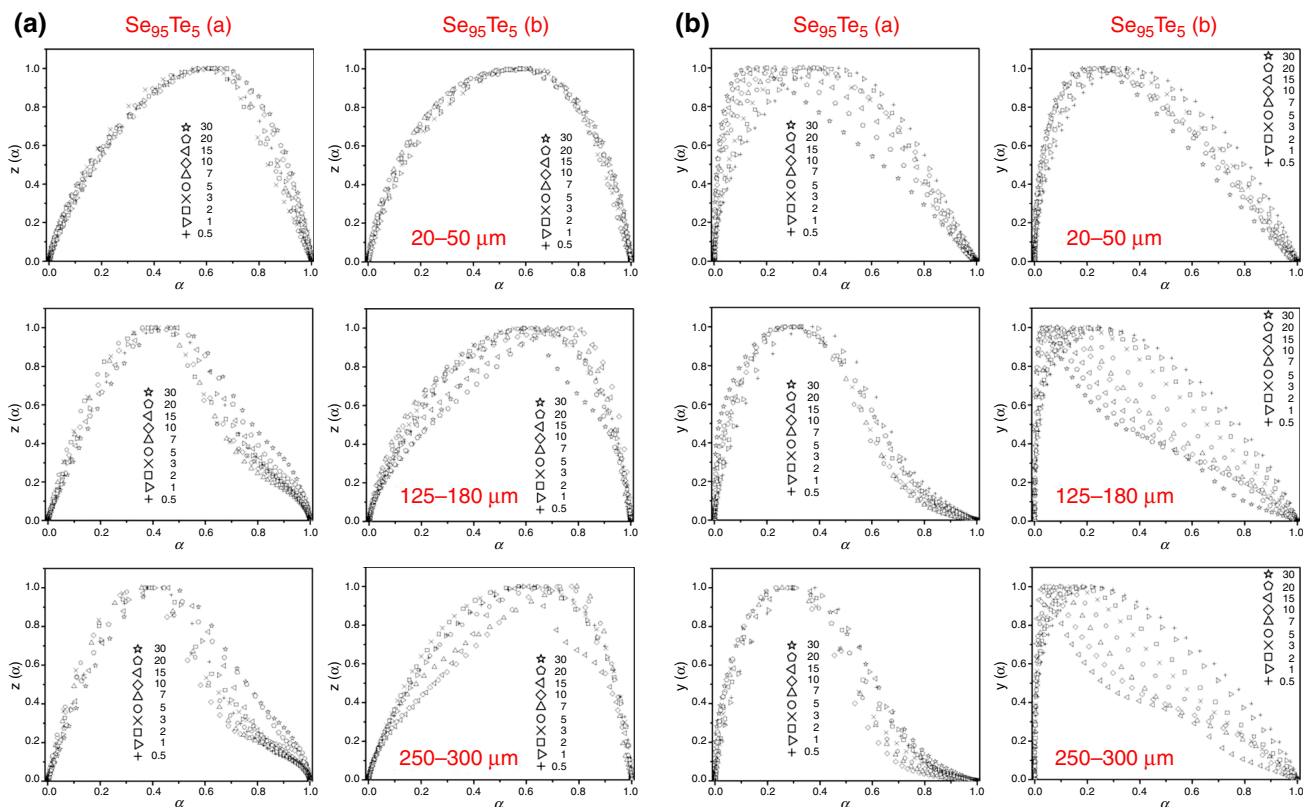


**Fig. 4** Characteristic kinetic functions corresponding to non-isothermal measurements of chosen particle size fractions of the  $\text{Se}_{95}\text{Te}_5$  glass—particular rows match the individual studied fractions. In the

left part **a** the data for  $z(\alpha)$  functions are displayed; right part **b** contains data for  $y(\alpha)$  functions. In each part respective columns corresponding to the data for batches (a) and (b) are shown

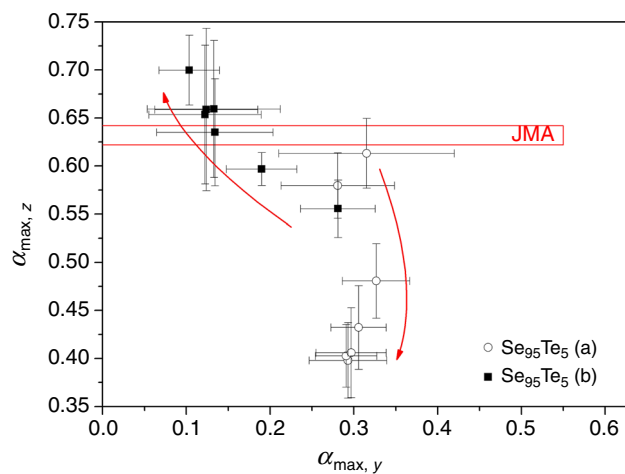


**Fig. 5** Kinetic plot evaluated for the two prepared  $\text{Se}_{95}\text{Te}_5$  glasses. Theoretical applicability of the JMA model as suggested by Málek [18] is displayed. Empty symbols correspond to the hyperquenched glass (a); gray symbols represent the data for the normally quenched glass (b). The arrows guide the eyes in the direction of the increasing particle size fraction within the particular glass batches

remaining position on the temperature axis, suggest a similar JMA mechanism being valid for this crystallization process originating from the microstructural stress-induced

defects formed within the material during glass-formation. It is only the peak tail (possibly corresponding to the last stages of the transformation of the amorphous phase occurring between the already crystalline parts of the grain), which causes the observed overall deviation.

In the last step of the kinetic analysis, the pre-exponential factor  $A$  and crystallization enthalpy  $\Delta H$  have to be determined. To determine the pre-exponential factor, the kinetic model with the corresponding parameters usually needs to be determined first; hence, again in the case of the data for  $\text{Se}_{95}\text{Te}_5$  glass, only those for the finest powders of batch (a) and low heating rates of batch (b) could be described—the value of pre-exponential factor was found to be  $\ln(A/s) = 36.8 \pm 0.2$ . Determination of the crystallization enthalpy is, on the other hand, possible for any data distorted by any means. Values of crystallization enthalpy (in  $\text{J g}^{-1}$ ) are compared in Fig. 6 for the two studied glass batches. The contour plots show the dependencies of  $\Delta H$  on heating rate  $q^+$  and averaged particle size for each powder fraction  $d_{\text{aver}}$  (bulk was assigned a value of  $1,000 \mu\text{m}$ ). Scaling is the same for the two plots; the white area corresponds to the measurements where the crystallization peak has already merged with (or was influenced by)

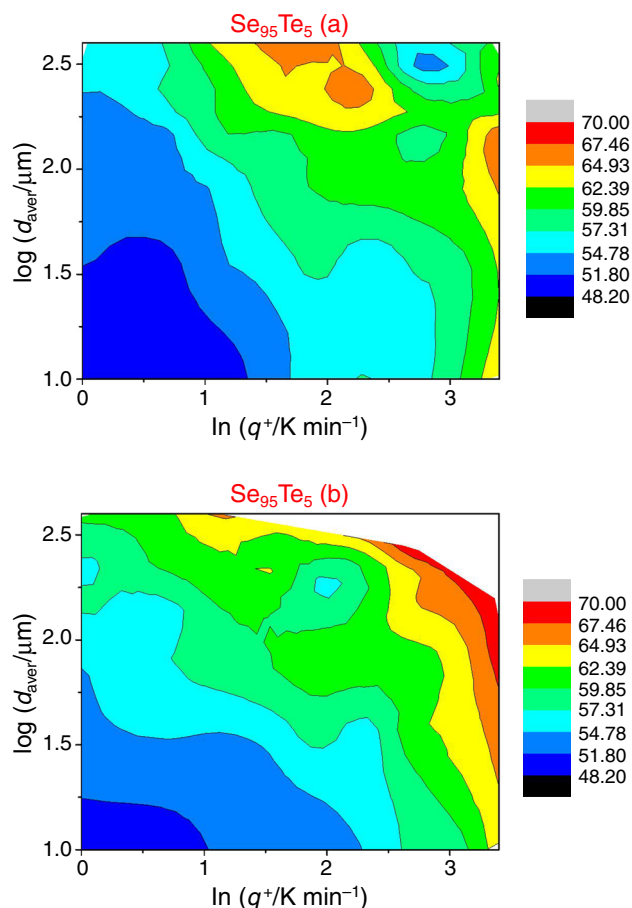


**Fig. 6** The overall crystallization enthalpy  $\Delta H_{\text{cry}}$  evaluated in dependence on heating rate and averaged particle size for the two prepared  $\text{Se}_{95}\text{Te}_5$  glass batches. Upper contour plot corresponds to the hyperquenched glass (a); lower contour plot represents the data for the normally quenched glass (b). Scaling of both plots is similar—suggested in the right part of figure. The white area in the plots suggest the “immeasurable” region where the crystallization process starts to merge with the consequent melting

the closely following melting. From the comparison of both plots, it can be seen that both crystallization mechanisms embody similar trends (as well as absolute values) in the development of  $\Delta H$ , which is well understandable as similar amounts of compositionally similar products are being formed. Incidentally, these trends seem to have general validity for crystallization processes non-isothermally measured by DSC—more on this point can be found in [7], where the involved physical principles are described.

As was shown in the previous paragraphs, in the case of certain types of process complexity, the standard kinetic analysis as well as advanced interpretation of characteristic kinetic functions [2, 6] fail. A suitable answer may be provided either by relatively tedious deconvolution procedures [5] or by a simple qualitative interpretation of the shapes of the DSC crystallization peaks. In both cases, however, it is the study performed in dependence on the

particle size which provides essential information on the studied crystallization kinetics.

#### Fraser–Suzuki deconvolution

Kinetic analysis of complex processes experienced significant progress recently. One of the most important tools in this regard is the (modified) Fraser–Suzuki deconvolution procedure [5, 23]. In the following text this helpful tool will be utilized to reveal details about the crystallization processes occurring in the  $\text{Se}_{95}\text{Te}_5$  glass. The Fraser–Suzuki deconvolution employs the following function in order to meaningfully separate overlapping kinetic processes:

$$y = a_0 \exp \left[ - \ln 2 \left[ \frac{\ln \left( 1 + 2a_3 \frac{x-a_1}{a_2} \right)}{a_3} \right]^2 \right] \quad (5)$$

where  $a_0$ ,  $a_1$ ,  $a_2$ , and  $a_3$  are the parameters corresponding to the amplitude, position, half-width, and asymmetry of the curve, respectively.

First, the FS deconvolution was applied to data for the batch (a) glass. An example deconvoluted curve is shown in Fig. 7. The deconvolution confirms that the overall material response is composed from two sub-processes (their envelope curve fits the experimental data very well). Properties and mutual position of the two peaks very well correspond to the conclusions derived on the basis of advanced peak shape analysis in Section 3.1. Namely the impingement-influenced crystal growth within the residual amorphous matrix well corresponds to the second (high-temperature) peak shape: marked positive asymmetry, elongated end tail, and onset corresponding with the maximum of the primary (preceding) crystallization process. The deconvolution also confirmed the already obvious unique independence of the primary crystallization process on particle size. The fact that the primary crystallization process is represented by only one peak (instead of the usual overlapping surface and volume peaks) suggests the presence of a strong driving force which surpasses that introduced mechanically during preparation of powders. In other words, this influence unifies the material properties, results in high density of crystallization centers and lowers the kinetic barriers for crystal formation so that the further introduction of mechanical defects and structural heterogeneities during powder grinding is of minor significance. As suggested in Section 3.1, this unifying influence is most probably the high amount of stress-induced defects formed within the original bulk material prepared by hyperquench.

Alternative hypotheses for the above-described behavior are: that it is caused by grinding-induced formation of crystallites or that some crystalline centers were formed already during the glass formation. Both these options are



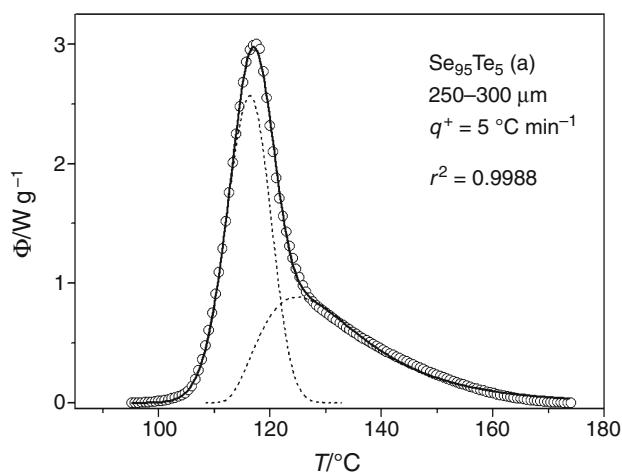


**Fig. 7** Example of batch *a* crystallization peak deconvolution performed using the Fraser–Suzuki function. Identification of the curve as well as correlation coefficient is given in the graph. Points, solid lines, and dotted lines correspond to the experimental data, overall fit, and particular deconvoluted peaks, respectively

of very low probabilities because in such cases there would still occur marked dependence of crystallization behavior on particle size and two intrinsic crystallization processes (“surface” and bulk) could be identified. In addition, in order for the process to be so perfectly unified an enormous amount of crystalline centers would have to be formed in the original glassy material, which would be recognized by the XRD analysis. The XRD analysis was performed on a very finely powdered material, so the potential effect of grinding-induced crystallization would be recognized too.

Fraser–Suzuki deconvolution applied to the glass batch (b) also revealed an interesting behavior, namely that in case of higher heating rates and middle-sized and coarse powder fractions an additional crystallization mechanism starts to occur. Example deconvoluted batch (b) data are shown in Fig. 8. As can be seen, apart from the usual “surface” and bulk crystallization peaks (black dashed curves; “surface” crystallization peak is the smaller one) there is a third, relatively small peak (red dashed curve; marked by arrow). While both the usually observed processes (“surface” and bulk crystallization) behave similarly as was observed for e.g., a-Se [6, 7] or Se–Te alloys [1–5], the third process is very precisely localized in temperature with respect to both—heating rate and particle size. The localization with respect to heating rate simply means that the process has very high apparent activation energy. The localization with respect to the particle size, on the other hand, markedly resembles the primary crystallization mechanism manifesting in case of glass batch (a). Due to the high activation energy the third process occurs only in case of those measurements, where significant portion of material is in amorphous state at  $\sim 165$  °C (i.e.,

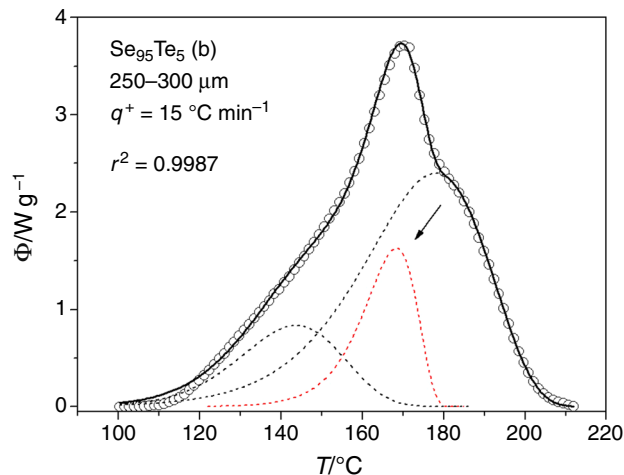
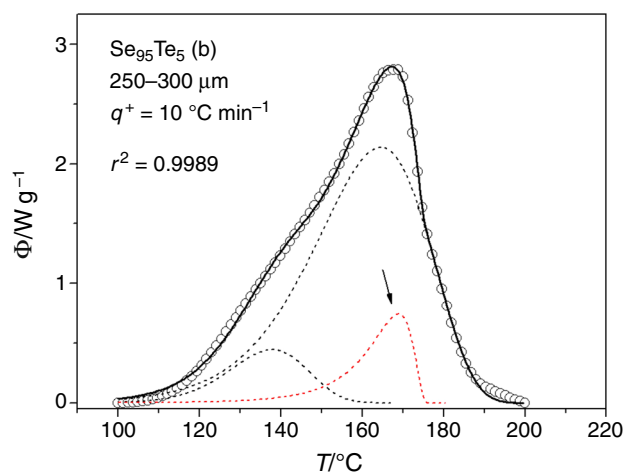


**Fig. 8** Examples of deconvoluted curves for batch (b) glass; deconvolution was performed using the Fraser–Suzuki function. Identification of the curves as well as correlation coefficients is given in the graphs. Points, solid lines, and dotted lines correspond to the experimental data, overall fit, and particular deconvoluted peaks, respectively. The red peak marked by arrow corresponds to the newly identified “third” type of crystallization mechanism

in case of high heating rates or coarse powder fractions). This is well apparent in Fig. 9 where the raw DSC data for the 300–500  $\mu\text{m}$  fraction are depicted (in this figure the effect of the crystallization process merging with the closely following melting can also be seen). The marked independence of the third process on particle size is then well apparent from Fig. 3, as already discussed in the respective article section.

The marked resemblance between the primary process manifesting in case of the hyperquenched glass and the “third” process occurring for the batch (b) glass leads to a conclusion that both processes are of a similar nature. In case of the batch (b) glass the process probably manifests in its true nature—given the corresponding high apparent activation energy. In case of the hyperquenched glass it is

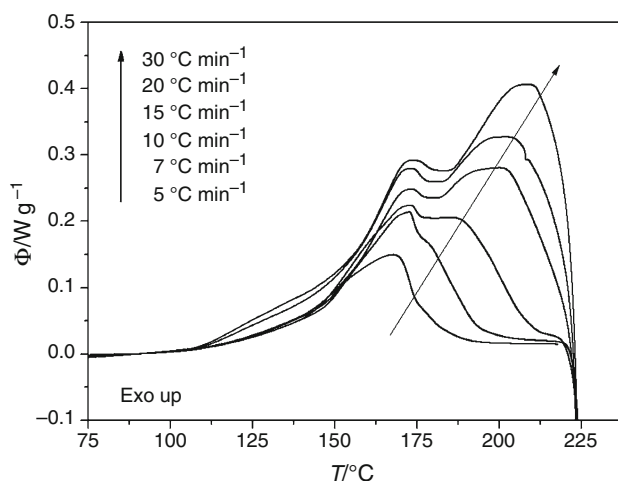


**Fig. 9** Raw DSC data for the 300–500  $\mu\text{m}$  particle size fraction of the batch (b) glass

probably the high amount of stress-induced defects, which significantly lowers the energetic barriers for crystal formation, thus shifting the crystallization process to lower temperatures where it exhibits a usual dependence on heating rate (providing a value of apparent activation energy of crystallization typical for Se–Te chalcogenide materials). Proposal on the possible structural origin of the above-discussed new crystallization mechanism will be introduced in the following section.

#### Structural origin of the “third” mechanism

Recent systematic research of the crystallization kinetics in the Se–Te glassy system revealed that the activation energy for the overall crystallization process gradually decreases with decreasing Te content [4, 6]. The deconvolution studies, however, showed that activation energy for the minor process of “surface” crystallization significantly increases with decreasing Te content (while in the case of pure Se both activation energies—of bulk and “surface” processes—are again very similar). This rising difference between activation energies of the two involved mechanisms  $\Delta E$  (major bulk crystallization and minor “surface” crystallization) leads to their partial separation, which starts to be well recognizable for the finest powder fractions of the  $\text{Se}_{90}\text{Te}_{10}$  composition. Considering the above-mentioned trend, together with the fact that for pure Se both activation energies are again similar, a sharp transition in the  $\Delta E$  quantity may be expected around the  $\text{Se}_{95}\text{Te}_5$  composition. This hypothesis is further supported by recent structural relaxation studies [24, 25], which revealed a marked sharp increase in the non-exponentiality parameter within the 0–10 at% Te compositional range (see Fig. 10).

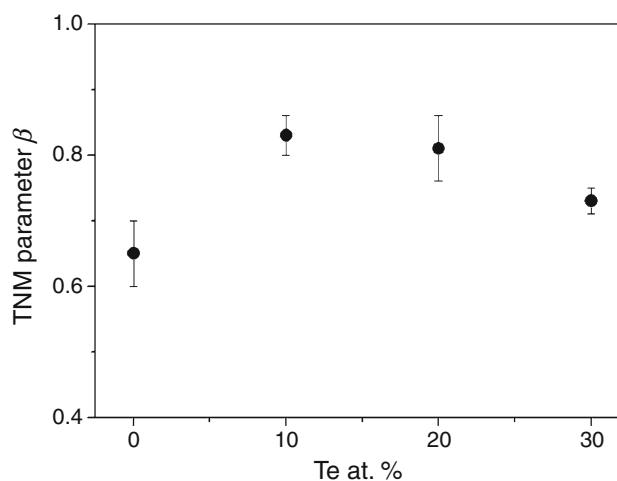


**Fig. 10** Dependence of the non-exponentiality parameter  $\beta$  (evaluated within the Tool-Narayanaswamy-Moynihan structural relaxation model) on Te content in the Se–Te chalcogenide glasses

This parameter expresses the width of the relaxation times distribution and is often associated with a measure of the degree of segmental cooperativity. Its sharp increase signifies a structurally distinct compositional region that may exhibit extreme behavior (anomalous trends were observed e.g., for viscosity and microhardness [26]).

Data presented in the current article show a marked difference between the crystallization kinetics of the normally quenched and hyperquenched  $\text{Se}_{95}\text{Te}_5$  glasses. Such divergence was not observed for any other studied Se–Te composition. Thorough studies of the effect of the annealing temperature during the glass preparation were performed for  $\text{Se}_{70}\text{Te}_{30}$  [2] (tested temperatures were 450 and 650 °C) and pure Se (results not published, tested temperatures were 350 and 650 °C)—in both cases no significant change in crystallization kinetics was recorded. A similar conclusion can also be derived for the  $\text{Se}_{80}\text{Te}_{20}$  and  $\text{Se}_{90}\text{Te}_{10}$  compositions, for which varying amounts of microstructural strain were applied during the preparation of additional glass batches assigned for reproducibility measurements. From this point of view, the reported effect of hyperquenching on crystallization kinetics also seems to be a rather structurally based compositional anomaly.

It is well known that the glassy structure in the Se–Te system is formed by a mixture of Se–Te chains and rings with a significant fraction of heteropolar bonding, where the tellurium atoms seem to be distributed more or less randomly within the selenium chains [27–29]. Correspondingly, no phase separation region occurs in the Se–Te glassy system—both elements are reported to mix in any ratio [30]. In the crystalline form all the Se–Te alloys compose a hexagonal lattice similar to that of pure Se and

Te; correspondingly to the particular compositions, the lattice parameters gradually change between the two extremes represented by Se and Te. Bearing the above mentioned in mind, it leaves the joint effect of the Se–Te chain length and the strength/quantity of the van der Waals forces interconnecting the neighboring chains as a possible reason for the anomalous behavior reported in the current article. In particular, the high degree of cooperativity and interlinking expected for the  $\text{Se}_{95}\text{Te}_5$  glass (based on the compositional dependence of relaxation non-exponentiality [24, 25]) may be responsible for slower release of stress and strain accumulated in the material during the hyperquenched glass formation, which in consequence leads to irreversible formation of microstructural defects. For a small number of large cooperatively relaxing clusters the stress would not be distributed uniformly and the formation of defects could then be localized at an interface between structurally diverse segments.

## Conclusions

Three types of crystallization mechanism were found to occur in Se–Te glasses. The first two mechanisms are well known: bulk crystallization originating from nuclei randomly distributed in the volume of each glass particle (formation of these nuclei is consistent with the classical nucleation theory) and crystallization from surface/volume active centers, dislocations, structural defects, and heterogeneities originating from the mechanical damage of the material (e.g., during grinding and milling). Manifestation of the third mechanism, on the other hand, appears to be rare for the Se–Te system—it was observed only for the  $\text{Se}_{95}\text{Te}_5$  composition. The most striking aspect of its evincing is its marked independence from particle size. The origin of this mechanism seems to be closely associated with the stress-induced defects formed within the highly stressed structures of hyperquenched glasses. The strong compositional dependence of the occurrence of this mechanism is then possibly caused by the high cooperativity of the amorphous structure of the specific composition.

In addition to the identification of the new crystallization mechanism, the difficulty of performing the kinetic calculations in the case of certain partially overlapping complex processes was discussed. As was shown, the advanced interpretation of characteristic kinetic functions fails in this case; besides the decisive (modified) Fraser–Suzuki deconvolution, the interpretation of the shape of crystallization peaks themselves provides a viable option for preliminary kinetic analysis.

**Acknowledgements** This work has been supported by the Czech Science Foundation under project No. P106/11/1152.

## References

1. Svoboda R, Krbal M, Málek J. Crystallization kinetics in Se–Te glassy system. *J Non Cryst Sol.* 2011;357:3123–9.
2. Svoboda R, Málek J. Interpretation of crystallization kinetics results provided by DSC. *Thermochim Acta.* 2011;526:237–51.
3. Barták J, Svoboda R, Málek J. Electrical conductivity and crystallization kinetics in Te–Se glassy system. *J Appl Phys.* 2012;111:094908.
4. Svoboda R, Málek J. Extended study of crystallization kinetics for Se–Te glasses. *J Therm Anal Calorim.* 2013;111:161–71.
5. Svoboda R, Málek J. Applicability of Fraser–Suzuki function in kinetic analysis of complex crystallization processes. *J Therm Anal Calorim.* 2013;111:1045–56.
6. Svoboda R, Málek J. Crystallization kinetics of a-Se, part 1: interpretation of kinetic functions. *J Therm Anal Calorim.* 2013;114:473–82.
7. Svoboda R, Málek J. Crystallization kinetics of a-Se, part 2: deconvolution of a complex process—the final answer. *J Therm Anal Calorim.* 2013;115:81–91.
8. Svoboda R, Málek J. Particle size influence on crystallization behavior of  $\text{Ge}_2\text{Sb}_2\text{Se}_5$  glass. *J Non Cryst Sol.* 2012;358:276–84.
9. Svoboda R, Málek J. Description of macroscopic relaxation dynamics in glasses. *J Non Cryst Solids.* 2013;378:186–95.
10. Svoboda R, Málek J. Enthalpy relaxation in Ge–Se glassy system. *J Therm Anal Calorim.* 2013;113:831–42.
11. Svoboda R, Málek J. Structural relaxation in Se-rich As–Se glasses. *J Non Cryst Solids.* 2013;363:89–95.
12. Šesták J. Thermophysical properties of solids, their measurements and theoretical analysis. Amsterdam: Elsevier; 1984.
13. Kissinger HE. Reaction kinetics in differential thermal analysis. *Anal Chem.* 1957;29:1702–6.
14. Svoboda R, Málek J. Is the original Kissinger equation obsolete today? *J Therm Anal Calorim.* 2014;115:1961–7.
15. Ryschenkow G, Faivre G. Bulk crystallization of liquid selenium. *J Cryst Growth.* 1988;87:221–35.
16. Bisault J, Ryschenkow G, Faivre G. Spherulitic branching in the crystallization of liquid selenium. *J Cryst Growth.* 1991;110:889–909.
17. Málek J. Kinetic analysis of crystallization processes in amorphous materials. *Thermochim Acta.* 2000;355:239–53.
18. Málek J. The kinetic analysis of non-isothermal data. *Thermochim Acta.* 1992;200:257–69.
19. Avrami M. Kinetics of phase change I—general theory. *J Chem Phys.* 1939;7:1103–12.
20. Avrami M. Kinetics of phase change. II—transformation-time relations for random distribution of nuclei. *J Chem Phys.* 1940;7:212–24.
21. Avrami M. Granulation, phase change, and microstructure—kinetics of phase change III. *J Chem Phys.* 1941;7:177–84.
22. Johnson WA, Mehl KF. Reaction kinetics in processes of nucleation and growth. *Trans Am Inst Min (Metall) Eng.* 1939;135:416–42.
23. Perejón A, Sánchez-Jiménez PE, Criado JM, Pérez-Maqueda LA. Kinetic analysis of complex solid-state reactions. A new deconvolution procedure. *J Phys Chem B.* 2011;115:1780–91.
24. Svoboda R, Honcová P, Málek J. Enthalpic structural relaxation in Te–Se glassy system. *J Non Cryst Solids.* 2011;357:2163–9.
25. Svoboda R. Relaxation processes in selenide glasses: effect of characteristic structural entities. *Acta Mater.* 2013;61:4534–41.

26. Kozyukhin SA. Anomalous mechanical properties of tellurium-modified glassy selenium. *Neorg Mater.* 2006;42:210–4.
27. Venugopal RK, Bhatnagar AK. Electrical and optical studies on amorphous Se–Te alloys. *J Phys D Appl Phys.* 1992;25:1810–6.
28. Zhao G, Zhao Y, Wang Y, Ji CJ. Ab initio molecular dynamics study of liquid  $\text{Se}_{30}\text{Te}_{70}$ : structural, electronic and dynamic properties. *Phys Scr.* 2010;82:035603.
29. El-Korashy A, El-Zahed H, Radwan M, Abdalla AM. Influence of composition and heat treatment on the structure of Se–Te films. *Thin Solid Films.* 1995;261:328–33.
30. Borisova ZU. *Glassy semiconductors.* New York: Plenum Press; 1981.